The H channel is not a proton transfer path in yeast cytochrome c oxidase

Malkamäki, Aapo

2019-09-01

Malkamäki , A , Meunier , B , Reidelbach , M , Rich , P R & Sharma , V 2019 , ' The H channel is not a proton transfer path in yeast cytochrome c oxidase ' , Biochimica et Biophysica Acta. Bioenergetics , vol. 1860 , no. 9 , pp. 717-723 . https://doi.org/10.1016/j.bbabio.2019.07.012

http://hdl.handle.net/10138/304661
https://doi.org/10.1016/j.bbabio.2019.07.012

BBA - Bioenergetics 1860 (2019) 717–723

Contents lists available at ScienceDirect

BBA - Bioenergetics

journal homepage: www.elsevier.com/locate/bbabio

The H channel is not a proton transfer path in yeast cytochrome *c* oxidase

Aapo Malkamäki[a], Brigitte Meunier[b], Marco Reidelbach[a], Peter R. Rich[c,*], Vivek Sharma[a,d,**]

[a] Department of Physics, P. O. Box 64, University of Helsinki, 00014 Helsinki, Finland
[b] Institute for Integrative Biology of the Cell (I2BC), CEA, CNRS, Université Paris Sud, Université Paris Saclay, 91198 Gif sur Yvette, France
[c] Department of Structural and Molecular Biology, University College London, Gower Street, London WC1E 6BT, UK
[d] Institute of Biotechnology, P. O. Box 56, University of Helsinki, 00014 Helsinki, Finland

ARTICLE INFO

Keywords:
Electron transfer
Proton pumping
MD simulations
Cell respiration
Mitochondria

ABSTRACT

Cytochrome *c* oxidases (CcOs) in the respiratory chains of mitochondria and bacteria are primary consumers of molecular oxygen, converting it to water with the concomitant pumping of protons across the membrane to establish a proton electrochemical gradient. Despite a relatively well understood proton pumping mechanism of bacterial CcOs, the role of the H channel in mitochondrial forms of CcO remains debated. Here, we used site-directed mutagenesis to modify a central residue of the lower span of the H channel, Q413, in the genetically tractable yeast *Saccharomyces cerevisiae*. Exchange of Q413 to several different amino acids showed no effect on rates and efficiencies of respiratory cell growth, and redox potential measurements indicated minimal electrostatic interaction between the 413 locus and the nearest redox active component heme *a*. These findings clearly exclude a primary role of this section of the H channel in proton pumping in yeast CcO. In agreement with the experimental data, atomistic molecular dynamics simulations and continuum electrostatic calculations on wildtype and mutant yeast CcOs highlight potential bottlenecks in proton transfer through this route. Our data highlight the preference for neutral residues in the 413 locus, precluding sufficient hydration for formation of a proton conducting wire.

1. Introduction

Mitochondrial cytochrome *c* oxidase (CcO) is a member of the A1 branch of the haem-copper oxidase (HCO) superfamily of respiratory oxidases that catalyse the four-electron reduction of molecular oxygen to water, conserving the free energy in the transmembrane proton electrochemical gradient [1–3]. Electrons are donated by cytochrome *c* to a dicopper centre (Cu_A) in subunit II and transferred to the O_2 reducing binuclear centre (BNC; composed of heme a_3 and a copper atom, Cu_B) in subunit I *via bis*-histidine coordinated heme *a*. Each electron transfer from heme *a* into the BNC is coupled to the uptake of two protons from the mitochondrial matrix: one pumped proton, ultimately translocated across the membrane, and one substrate proton directed into the BNC [4,5]. These protons traverse the interior of the largely hydrophobic enzyme along hydrophilic channels formed by arrays of protonatable/polar residues and associated water molecules [6,7]. Three such arrays, the D, K and H channels, have been identified within subunit I of both mitochondrial (bovine) and bacterial A1-type CcOs [8,9]. In bacterial A1-type HCOs, a large body of kinetic and mutant data indicates that the D and the K channels provide the route for substrate protons at different stages of the catalytic cycle, and that the D channel provides part of the pathway for all pumped protons [4,10]. Effects of mutations of channel residues in yeast mitochondrial CcO also support this view [11–14]. These studies have led to a mechanism with key features as follows [4,5]: electron transfer from haem *a* into the BNC is coupled with a proton transfer from E242 (bovine numbering) at the top of the D channel *via* a gated route into a proton trap region in the vicinity of the bound Mg^{++} or Mn^{++} ion above the BNC [15,16]. E242 is reprotonated from the N phase *via* the D channel. The opposite charges of the trap proton and the BNC electron stabilise each other. However, this electron transfer creates a protonatable site with a high pK_a within the BNC which becomes protonated *via* the K or D channel. This neutralises the negative charge in the BNC, destabilising the trap proton which is driven into the P phase *via* a gated route that has not yet been well defined.

All A-type CcOs also have a third structure, the H channel [18,19], though with some variations, and in the homologous A-type quinol oxidases, such as *E. coli* cytochrome bo_3, the majority of hydrophilic H

Abbreviations: CcO, cytochrome *c* oxidase; MD, molecular dynamics

* Correspondence to: P.R. Rich, Department of Structural and Molecular Biology, University College London, Gower Street, London WC1E 6BT, UK.
** Correspondence to: V. Sharma, Department of Physics, P. O. Box 64, University of Helsinki, 00014 Helsinki, Finland.
E-mail addresses: prr@ucl.ac.uk (P.R. Rich), vivek.sharma@helsinki.fi (V. Sharma).

https://doi.org/10.1016/j.bbabio.2019.07.012
Received 4 March 2019; Received in revised form 24 June 2019; Accepted 29 July 2019
Available online 30 July 2019

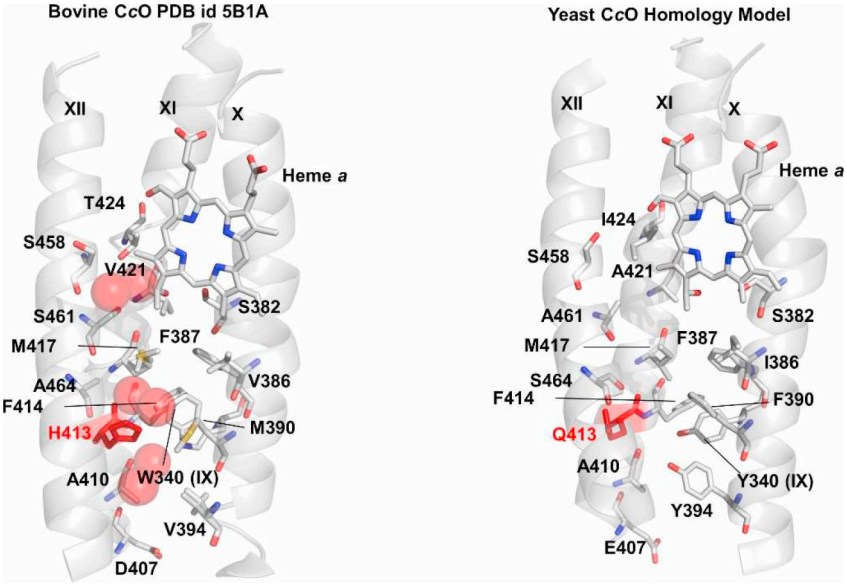

Fig. 1. Comparison of the 'lower' span of the H channel in bovine and yeast mitochondrial CcOs. Figures are drawn with atomic coordinates from PDB id 5B1A (oxidised bovine CcO, left) and the homology model of yeast CcO (right). Key H channel residues H413 (bovine)/Q413 (yeast) are shown in red and other amino acids that face the H channel pore are shown with atom-based colouring – red, oxygen; blue, nitrogen and white, carbon. Crystallographically-defined water molecules in this region of bovine CcO are shown as red spheres. See also Fig. S1 for comparison of the yeast CcO homology model and its structure in the recently solved cryo-EM model of the yeast III_2IV_2 supercomplex [17].

channel residues are replaced by aliphatics [20]. The H channel in A-type CcOs potentially connects the N and P phases, running past the hydroxyethylfarnesyl and formyl substituents of low spin haem *a* [9]. Structural and functional data from bovine CcO have provided evidence that it provides the pathway for pumped protons both into and out of the trap site in mammalian mitochondrial CcOs (reviewed in [19]). Specifically, a water/hydronium channel leads from the N phase at D407 *via* H413 towards haem *a*, gated by a redox- and ligand-sensitive movement of S382 [19,21,22] (see Fig. 1 for a comparison of this span in bovine and yeast CcOs). When the BNC reaches the R state (both metals reduced before oxygen binds [4,5]), S382 moves into helix X. This opens the channel, enabling four protons from the N phase to move to residues around heme *a*, and from there to the proton trap site around the bound Mg^{2+} *via* a short pathway involving R438/R439 [23]. The driving force for this accumulation of four protons in the trap site, particularly in the presence of a high protonmotive force, remains difficult to envisage. Nevertheless, it is suggested that subsequent binding of oxygen at the active site to form the oxyferrous intermediate A causes S382 to move out of helix X and block the transfer of protons back into the N phase. Protons are subsequently driven out of the trap into the P phase, one with each of the four electron transfers from heme *a* into the BNC that regenerate the R intermediate. The proton exit path into the P phase was proposed to run *via* R438/R439 through the hydrated 'top' part of the H channel that includes the Y440/S441 peptide bond and D51 at the P phase subunit I/II interface [24]. In this model of proton pumping, the substrate protons are still transferred *via* D and/or K channels, but they do not electrostatically influence the pumped protons in the trap, in contrast to the model described above.

Experimental testing of H channel function in mammalian CcOs is challenging, particularly because of the difficulty in generating well-defined mutants for direct functional, biochemical and biophysical studies. We have addressed the issue with atomistic molecular dynamics (MD) simulations of bovine CcO [25]. We showed that the lower part of the H channel around H413 could not hydrate sufficiently to form a proton-conducting pathway unless H413 could form its charged imazolium (q = +1) state, which appeared unlikely based on its predicted pK_a [25]. However, issues remain as to whether an electrostatic interaction with heme *a* could raise the pK_a of H413 when heme *a* becomes transiently reduced to enable proton transfer, or whether alterations around locus 413 could influence heme *a* properties and hence catalytic turnover. In this work, we focus on the same lower span of the H channel of yeast CcO, which is structurally very similar to that in bovine CcO (Fig. 1). Whereas a histidine occupies locus 413 in both bovine and bacterial CcOs, in yeast it is a glutamine (Q413; Fig. 1). To further characterize this region, we constructed and experimentally investigated several yeast CcO Q413 mutants and performed microseconds of atomistic MD simulations and continuum electrostatic calculations on yeast CcO model systems. The goals were to examine its hydration level in relation to a possible proton transfer route and to test whether interactions could occur between heme *a* and protonatable residues introduced into the 413 locus. The exchange of Q413 to polar and potentially charged residues H, K or E had no major effect on the enzymatic activity or on the redox properties of heme *a* and MD simulations confirmed the poor hydration of the region and the preference for neutral forms of all residues in the 413 locus, as in bovine CcO. Overall, these data show that this lack of net charge at locus 413 (Q413 in WT yeast CcO, neutral H413 in bovine CcO), regardless of the heme *a* redox state, precludes sufficient hydration to create an H-bonded pathway for proton transfer from the N phase towards haem *a* and the onward connectivity into the proton trap region.

2. Materials and methods

2.1. Yeast mutant constructs and mitochondrial membrane preparation

Yeast extract was purchased from Ohly GmbH, Germany. All other reagents were purchased from Sigma Aldrich. Yeast *Saccharomyces cerevisiae* strains were constructed from a modified strain W303-1B (Alpha *ade2 HIS3 leu2 trp1 ura3*) that expressed wild type CcO with a 6-his tag sequence attached to *Cox13* for ease of CcO purification. Protocols for construction of mutant forms of CcO with single point mutations of Q413H/K/E/L in the mitochondrial DNA-encoded subunit Cox1, growth of the yeast cells in galactose-containing medium and preparation of mitochondrial membrane fragments were as detailed in [13]. Mitochondrial membranes were stored at −80 °C in 50 mM potassium phosphate, 2 mM potassium EDTA at pH 7.4.

2.2. Turnover numbers of mutant strains

CcO concentrations were measured from sodium dithionite-reduced *minus* oxidised difference spectra at 604–619 nm with an extinction coefficient, Δε, of 26 $mM^{-1}.cm^{-1}$ (based on values for 606–621 nm of bovine CcO [26]). Steady-state oxygen consumption rates were measured in a stirred reaction vessel of a Clark-type O_2 electrode at 25 °C. Assays were carried out using mitochondrial membranes containing 2–10 nM CcO in 10 mM potassium phosphate at pH 6.6, 50 mM KCl,

0.05% (*w/v*) DDM, 2 mM sodium ascorbate and 40 μM TMPD [27]. A baseline was measured in the absence of cyt *c* and the reaction was initiated by addition of 50 μM cyt *c*. Turnover numbers and rates are expressed in terms of the number of electrons transferred from cyt *c* per second per C*c*O (e.s^{-1}).

2.3. Redox potential determinations

Redox titrations of the 604 nm heme components (with approx. 80%/20% contributions from hemes *a* and a_3, respectively) were performed essentially as outlined in [28]. A buffer containing 0.1 M potassium phosphate, 1 mM EDTA and 50 μM riboflavin at pH 7.5 was bubbled with argon for 5 min before adding 2.5 μM horse heart cytochrome *c*, 0.05% *w/v* UDM and mitochondrial membranes to a concentration of ~0.25 μM C*c*O. The sample was maintained anoxic under an atmosphere of argon. The fully oxidised state was established by addition of 25 μM potassium ferricyanide. Stepwise reduction of the sample was achieved by photoreduction of riboflavin with series of flashes from a xenon flashlamp (EG&G FX-200; 15 μF/flash), delivered to both sides of the cuvette *via* lightpipes. After equilibration at each step, ambient potential, E_h, was calculated from the fractional reduction of cytochrome *c* at 550–542 nm using a midpoint value of +255 mV *versus* SHE. Full reduction was achieved at the end by addition of 2 mM sodium ascorbate. Fractional reduction of the 604 nm band was determined as the size of the 604 nm peak relative to the weighted average of reference points at 590 and 618 nm. A correction was made for the small contribution of cytochrome *c* at this wavelength triplet by subtraction of 0.0134 of the 550–542 nm absorbance change. For ease of comparison, data were approximated with a pair of equal sized $n = 1$ Nernstian components, though the detailed behaviour of this multicomponent interacting redox system is more complex [28,29].

2.4. Computational methods

We performed MD simulations on a small model system (core subunits I and II) of yeast C*c*O using coordinates predicted by homology modelling using bovine C*c*O coordinates [30]. During manuscript prepartion the structure of yeast C*c*O was resolved as part of the supercomplex [17,31]. See Fig. S1 for comparison between the homology model and the recently solved structure. Q413 of yeast subunit I (equivalent to H413 of bovine C*c*O) was altered (see Table 1) to H, K, E or D to represent the yeast C*c*O variants generated by site-directed mutagenesis (see above). A lipid-protein-solvent system was constructed using CHARMM-GUI and associated tools [32]. The protein model systems were embedded in a pure POPC lipid bilayer. All redox active components were modelled in their oxidised states using force field parameterization of Johansson et al. [33]. The high spin heme a_3 was ligated by a water molecule, and Cu_B with a hydroxide and with the catalytic tyrosine (Y245) in its anionic state [34]. Standard protonation states were used for all other amino acids, except subunit I residues E243, K319, and D364, which were patched neutral. CHARMM NTER and CTER patches were used, respectively, for all the N- and C-terminals and, CHARMM force fields were used for the protein, membrane, water, and ions [35,36].

Table 1
Model systems and simulation lengths. Subscript 'p' and 'n' denote protonated and neutral forms of residues, respectively.

Small (subunits I + II) yeast C*c*O models systems and their setup details		Simulation time (~μs)
Q	WT (Q413) (q = 0)	2
H_δ	Q413H mutant with His N_δ protonated (q = 0)	2
H_ε	Q413H mutant with His N_ε protonated (q = 0)	2
H_p	Q413H mutant with His doubly protonated (q = +1)	2
	Q413H mutant with His doubly protonated (q = +1) and restraints to prevent flipping of His.	2
D	Q413D mutant (anionic; q = −1)	2
D_p	Q413D mutant (protonated; q = 0)	2
E	Q413E mutant (anionic; q = −1))	1.6
K	Q413K mutant (protonated; q = +1)	2
K_n	Q413K mutant (neutral; q = 0)	2

An energy minimisation procedure was used for the constructed systems (2 × 50,000 steps with maximum force < 1000 kJ mol^{-1} nm^{-1}) before running a short equilibration run (0.2 ns). Berendsen barostat [37] and Nosé-Hoover thermostat [38,39] were used during the equilibration. GROMACS software [40] was used for all the MD simulations. By constraining bonds associated with hydrogen (using LINCS [41]) a time step of 2 fs was used. During production runs, Parrinello-Rahman barostat [42] and Nosé-Hoover thermostat were utilized. The simulation lengths are given in Table 1. Simulation trajectory analysis and visualization was performed with VMD software [43]. pK_a calculations were performed on simulation snapshots using PROPKA software [44].

To complement and consolidate our homology model-based MD simulations (Table 1), we performed additional simulations on a two subunit (I and II) model system constructed from the recently solved yeast C*c*O structure [17] with redox centres modelled in fully oxidised and in fully reduced states (see Table S1 for model systems and their simulation lengths). The oxygenous ligands of metal centers in the fully oxidised state were modelled as described above, whereas in the fully reduced state high spin heme a_3 and Cu_B were modelled without oxygenous ligands and catalytic Y245 in its neutral form. The protonation states of all other amino acids were as described above.

3. Results

3.1. Effects of yeast C*c*O Q413 mutations

Strains of yeast with point mutations of its C*c*O subunit I residue Q413 mutated to L, H, K or E were grown in a respiration-dependent ethanol medium in order to assess respiratory chain competence and efficiency (Fig. 2). In all cases, exponential phase growth rates and maximum cell densities were similar, showing that the whole cell respiratory chain activities and their growth efficiencies were not affected by the mutations and hence there are no indications of defective activity or proton pumping.

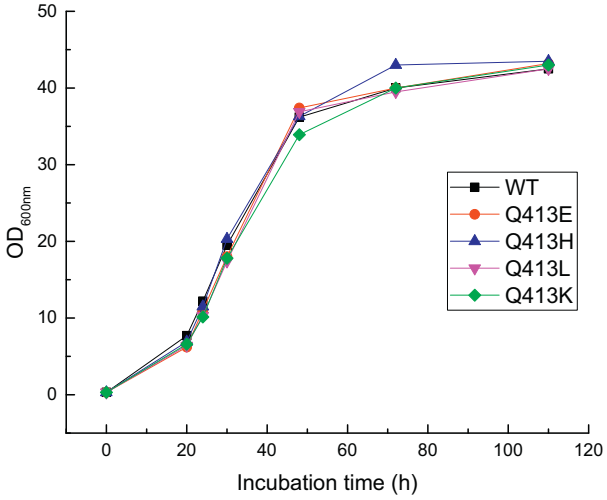

Fig. 2. Growth curves of WT and Q413 mutant yeast strains. Yeast WT and mutants were grown overnight on YPD plates (yeast extract 1%, peptone 2%, glucose 3%). Freshly grown cells were then inoculated at an initial OD_{600nm} of 0.3 in YPE medium (yeast extract 1%, peptone 2%, ethanol 2%) and cultivated at 28 °C with vigorous agitation. Cell densities were measured as OD_{600nm}. Diploids were used for the growth measurements.

For large batch cultures, cells were grown on YPGal medium and mitochondrial membranes were isolated as described in [13]. For all mutant strains, yields of mitochondria were similar. Reduced *minus* oxidised difference spectra were used to quantitate the levels of assembled respiratory complexes III and IV (C*c*O). The level of complex III per milligram of mitochondrial protein is always fairly constant in different C*c*O mutant strains. The levels of expressed C*c*O relative to Complex III were around 0.3–0.35 in WT and Q413H and 0.2–0.25 in the Q413E and Q413K variants. In all cases, the peak position of the heme A (largely representing heme *a*) in reduced *minus* oxidised difference spectra was the same as the WT at 604–5 nm, with no distortions or shoulders. Furthermore, all variants had turnover numbers similar to the WT value of ~1000 e.s^{-1} under the conditions of measurement. Overall, these data indicate that there could not have been a major structural or functional perturbation caused by these mutations.

It was of interest to determine whether changes at the Q413 locus could influence the midpoint potential of heme *a*, since a strong coupling would indicate that reduction of heme *a* could significantly raise the pK of a group in this locus. Redox titrations were performed as described in Methods. The major contributor to the 604 band is heme *a* (80%), with the remaining 20% arising from heme a_3 [26]. Both hemes titrate together, and redox interactions between them cause both to titrate in a complex manner with a high potential wave when the other heme is oxidised and a lower potential wave when the other heme is reduced. For comparative purposes, an approximate fit to the data was made with two $n = 1$ Nernstian components of equal size (Fig. 3), although the overall behaviour of the system is more complex, involving additional redox interactions with Cu_A and Cu_B [28,29]. An approximate fit to the WT data could be made with potentials of 320 mV and 245 mV (solid line in Fig. 3), representing primarily the high and low potential waves of heme *a* and are consistent with published data [45]. These heme *a* E_ms were little affected in the Q413H and Q413K mutants, and decreased only slightly by −15 to −20 mV in the Q413E mutant. Hence, there appears to be no strong electrostatic interaction between heme *a* and the residue at the 413 locus. Since the structure between heme *a* and the 413 locus is overall similar in yeast and bovine C*c*Os (Fig. 1), this indicates that there is also unlikely to be any large pK upshift of bovine H413 on heme *a* reduction, in agreement with our earlier calculations suggesting a mild increase in His413 pK_a by about

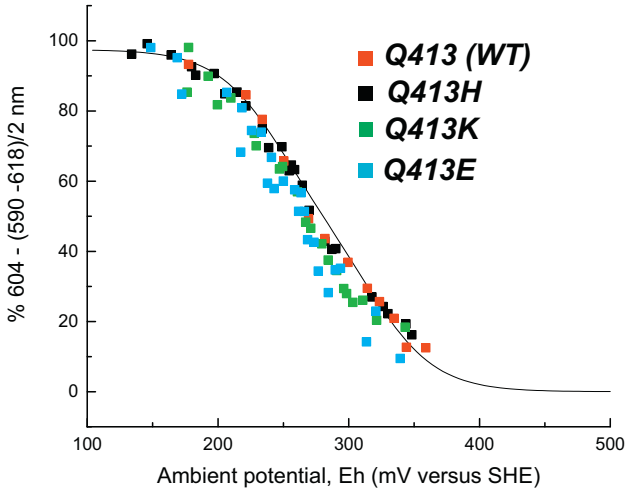

Fig. 3. Redox titrations of the 604 nm band of WT and mutant forms of yeast C*c*O in mitochondrial membranes. Mitochondrial membranes were suspended in an anaerobic buffer of 0.1 M potassium phosphate, 1 mM EDTA, 50 μM riboflavin, 2.5 μM horse heart cytochrome *c* and 0.05% *w/v* UDM at pH 7.5. Stepwise reduction of the 604 nm band of C*c*O was achieved by flash-induced reduction of the riboflavin and ambient redox potential was calculated from the redox poise of cytochrome *c*. Further details are given in Methods.

1–2 p*K* units on heme *a* reduction [25]. The distance from H413/Q413 to the macrocycle edge of heme *a* is ~13 Å (16.4 Å to heme *a* iron). If point charges were introduced at these distances with an intervening medium of dielectric constant of 4, large negative interaction energies of approx. 280 and 220 mV respectively would be predicted from the Coulombic electrostatics ($V = q_1.q_2/(4\pi\varepsilon_r\varepsilon_o r)$ where $q_1 = q_2 = 1.6 \times 10^{-19}$C, ε_r = dielectric constant of intervening medium, ε_o = vacuum permittivity = $8.8542 \times 10^{-12}C{\cdot}V^{-1}.m^{-1}$ and r = distance in m). The effective dielectric constant would have to be > 40 to reduce the interaction energy below −20 mV, which is unlikely given the structural details (Fig. 1). Instead, the small shifts indicate that the charge change on heme *a* is delocalised and counterbalanced by surrounding protein and water dipole adjustments as our prior simulations have suggested [25], and/or the altered residues are present in their neutral forms regardless of heme *a* redox state.

3.2. MD simulations of yeast C*c*O

MD simulations on the yeast WT C*c*O homology model with glutamine (Q) at position 413 indicate that there is insufficient hydration to form a protonic connection from the N phase at E407 towards A461 and the H channel residues around heme *a* (Fig. 4). Hence, as concluded previously for bovine C*c*O [25], proton transfer through this span by formation of an H-bonded wire appears improbable. Only when a charged residue replaces Q413 does this span gain additional water molecules to potentially create such a pathway. This is illustrated in Fig. S2, where replacement of Q413 with anionic (q = −1) aspartic acid, but not its neutral form, promotes an increased hydration that might provide such a pathway. The possibility of formation of such a water-facilitated proton path is explored in more detail in Table 2. This compares estimated pK_as and the simulated hydration states for residues Q, H, D, E and K at position 413 in their charged, uncharged and tautomeric forms. In the simulations of H, K and D in their neutral states, they remain buried in the hydrophobic protein interior, away

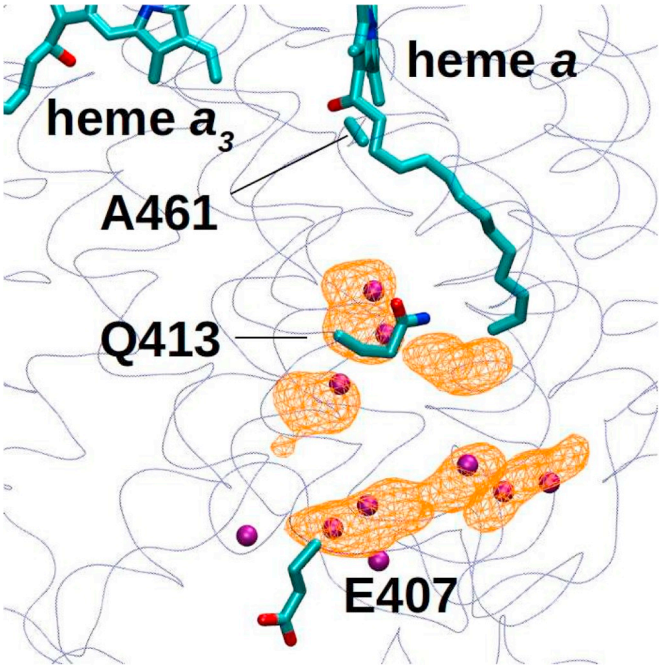

Fig. 4. Hydration in the lower part of H channel in yeast WT C*c*O simulations. Amino acids are shown with atom-based colouring (carbon – cyan; oxygen – red; nitrogen - blue) and polypeptide backbones are displayed as thin ribbons. The orange mesh represents average water occupancy calculated over the entire simulation trajectory and is plotted at an isovalue of 0.15, whereas instantaneous water oxygen atom positions are shown as purple spheres.

Table 2
Average pK_a, no. of water molecules and solvent exposure of amino acid at position 413 in yeast C*c*O simulations[a].

Model systems	pK_a of amino acid residue at 413 position (± std. dev.)	# Water molecules within 5 Å of residues at positions 461 and 413 (± std. dev.)	Buried (%)
Q (q = 0)	–	1.00 ± 0.65	–
H_δ (q = 0)	3.75 ± 0.24	0.05 ± 0.05	83
H_ε (q = 0)	4.28 ± 0.65	1.13 ± 0.68	69
H_p (q = +1)	3.89 ± 0.53	2.28 ± 0.98	80
D (q = −1)	4.88 ± 0.47 (6.14 ± 0.31 with > 70% buried)	3.73 ± 1.51	55
D_p (q = 0)	6.43 ± 0.29	0.89 ± 0.41	67
E (q = −1)	6.28 ± 0.47	0.59 ± 0.60	63
K (q = +1)	9.47 ± 0.96 (7.92 ± 0.75 with > 70% buried)	0.80 ± 0.63	25
K_n (q = 0)	7.10 ± 0.51	0.45 ± 0.80	93

[a] Average is calculated based on simulation snapshots selected every 20 ns. Buried (%) reveals how buried a charged residue at position 413 is in the hydrophobic interior of protein and is a measure of the percentage of the surface of the residue that is inaccessible to solvent, averaged from all snapshots. Subscript 'p' and 'n' denote protonated and neutral forms of residues, respectively.

from the solvent phase at the N side. In these cases, the pK_a calculations indicate that the uncharged state of the residue is stabilized and hydration between it and A461 remains low as is the case for WT Q413 (Table 2). Only when H and D substitutions are modelled in their charged states is increased hydration between it and A461 observed (D shown in Fig. S2). Interestingly, a different behaviour is observed when the charged state of the longer sidechain of K (and E) is modelled; it is able to reorient 'downwards' towards E407 where it is less buried and tends to recruit water molecules towards E407 and the N phase, though the span towards A461 remains poorly hydrated (Fig. S3). This results in a high pK_a of *ca.* 9.5 (Table 2) which stabilizes its charged state in this orientation. In simulation snapshots in which protonated K has not bent downwards (> 70% buried), pK_a estimates are downshifted to *ca.* 7–8, favouring its partly neutral state, similar to the pK_a estimates for the neutral K simulations where the sidechain always remains buried and less hydrated (Table 2 and Fig. S3).

Microseconds simulations on the wild type and mutant models constructed from the recent structure of yeast C*c*O [17], with redox centres fixed in the fully oxidised or fully reduced states, further consolidated our findings from the homology model-based MD simulations (see Tables S1, S2 and S3).

Importantly, two main conclusions emerge. First, we find that the neutral protonation states of titratable residues are stabilized at the 413 locus, which does not facilitate hydration of the lower span of the H channel. This is also the case for the WT where neutral Q is at this locus (Fig. 4). Second, the flipping and stabilization of the charged form of K or E (Fig. S3 and Tables 2, S2 and S3) towards E407 and the N phase also results in water occupancy of the span towards A461 that is insufficient for formation of a proton-conducting water wire. Overall, the simulation data are consistent with the experimental measurements showing that mutations of Q413 to H, K or E have no strong effect on heme *a* midpoint potential (Fig. 3), indicative of weak electrostatic coupling between the residue at position 413 and heme *a* and supporting the view that these residues do not form their charged states. Together with their lack of effects on oxygen reduction rates or cell growth efficiencies, the experimental and simulation data are overall consistent with the conclusion that this span does not provide the pathway for redox-coupled proton pumping in yeast C*c*O.

4. Discussion

Earlier we showed based on large-scale atomistic MD simulations that the upper (D51, Y54/, Y371, Y440 and S441) and middle (R38, T424, S454 and S458) parts of the proposed H channel in bovine C*c*O (connecting the region around heme *a* to the P aqueous phase) are sufficiently hydrated to create a possible proton transfer pathway towards the P side of the membrane [25]. However, this was not the case for its lower section that connects the N phase at D407 with the region up to S382/S461 and heme *a*. Specifically, with the centrally-placed H413 (see Fig. 1) simulated in a neutral singly-protonated (HSD) state, we did not see sufficient hydration to form a route for rapid proton transfer. Only when H413 was doubly protonated (imidazolium; q = +1) did additional hydration occur both above and below it to increase possibilities for protonic connectivity from the N phase to the middle and top spans of the H channel. However, continuum electrostatic calculations showed that the pK_a of H413 was too low (p$K_a \leq 5$) to favour its imidazolium form, hence bringing into question a possible proton pathway function of this span. Here we report simulations of this region of yeast mitochondrial C*c*O with several of the amino acid substitutions of its 413 locus that have been also been analysed experimentally by performing activity and redox potential measurements. The goal was to estimate its hydration level in relation to possible formation of a proton-conducting pathway and to test whether a strong electrostatic interaction could exist between this locus and heme *a*.

An extensive set of mutations have been introduced previously into the K, D and H channel regions of yeast C*c*O [13]. Effects on coupling ratio of a vesicle-reconstituted enzyme with four mutations in the H channel suggested that, like bacterial C*c*Os, coupling efficiency was not perturbed by such H channel interference [11]. Coupling efficiencies in yeast C*c*O with mutations of single residues in all three channels were also made by measurement of 'classical' H^+/O ratios in intact mitochondria [12,14] from state 3/4 transitions induced by ADP additions [46]. These confirmed the lack of H channel mutant effects and also showed that mutations in the D channel had effects similar to those found in bacterial C*c*Os, including uncoupling of proton translocation from oxygen catalysis in an N99D channel mutant whose bacterial equivalent (N139D in *R. sphaeroides* C*c*O) has the same effect [47,48]. The mutations of yeast C*c*O H channel residue Q413 reported here also failed to affect growth efficiency or turnover rates and introduction of potentially charged residues had little effect on the measured midpoint potential of heme *a*, suggesting weak electrostatic interaction between it and the residue in the 413 locus. The simulations of the homology-modelled structure of yeast C*c*O, as well as of models constructed from a recently-published cryo EM structure [17] provide further consistent data in this regard. The WT enzyme has a neutral glutamine residue at key locus 413. In this case, hydration above and below it is insufficient to create an H-bonded pathway for proton transfer. Modelling of histidine (or aspartic acid) at this locus increased hydration but only if simulated in its charged form. However, the pK_a estimates (Tables 2, S2 and S3) indicate that uncharged forms of residues, and hence low hydration, is the preferred state. Introduction of glutamic acid or lysine in their uncharged states had the same effect; however, the flexibility of their longer sidechains allowed their charged forms to orient more towards E407 and the N phase leading to the recruitment of waters towards E407. Notably, this stable 'downward' conformation still resulted in poor hydration above 413 locus and hence a major bottleneck for proton transfer through this route. Overall, the experimental and simulation data reinforce the conclusion that this channel in WT yeast C*c*O cannot provide a proton pathway, that the site anyway favours an uncharged residue, and that there is little electrostatic interaction

between residues placed at this locus and heme *a*. This latter point is relevant to bovine CcO which has a histidine in the 413 locus. A strong electrostatic interaction with heme *a* could stabilise its charged imidazolium state that we have proposed is a prerequisite for a hydrated proton pathway [25]; the overall similarity of the bovine and yeast structures in this region (Fig. 1) argues against such an effect. For both bovine and yeast CcOs, the question remains as to whether this section of the H channel could play a possible role of a dielectric well role. The lack of large electrostatic interaction between the 413 locus and heme *a*, together with the lack of observed redox- or ligand-induced structural effects tends to argue against this and instead the upper, more conformationally flexible span of the H channel may well be a more suitable candidate for transmission of allosteric effects to modulate heme *a* properties and influence catalytic parameters. Such control by other elements such as accessory subunits or small molecule binding will require further experimental investigation.

Transparency document

The Transparency document associated with this article can be found, in online version.

Acknowledgements

VS acknowledges research funding from the Academy of Finland (294652), the University of Helsinki and the Sigrid Jusélius Foundation. PRR was funded by BBSRC grants BB/K001094/1 and BB/L020165/1 and much of the redox potentiometry was performed by student Antonios Poulitsidis. *VS* is thankful to Center for Scientific Computing – IT Center for Science, Finland for computational support.

Appendix A. Supplementary data

Supplementary data to this article can be found online at https://doi.org/10.1016/j.bbabio.2019.07.012.

References

[1] J.A. García-Horsman, B. Barquera, J. Rumbley, J. Ma, R.B. Gennis, The superfamily of heme-copper respiratory oxidases, J. Bacteriol. 176 (1994) 5587.
[2] J. Hemp, R.B. Gennis, Diversity of the heme–copper superfamily in archaea: insights from genomics and structural modeling, in: G. Schäfer, H.S. Penefsky (Eds.), Bioenergetics: Energy Conservation and Conversion, Springer Berlin Heidelberg, Berlin, Heidelberg, 2008, pp. 1–31.
[3] F.L. Sousa, R.J. Alves, M.A. Ribeiro, J.B. Pereira-Leal, M. Teixeira, M.M. Pereira, The superfamily of heme–copper oxygen reductases: types and evolutionary considerations, Biochim. Biophys. Acta (BBA)-Bioenergetics 1817 (2012) 629–637.
[4] M. Wikström, K. Krab, V. Sharma, Oxygen activation and energy conservation by cytochrome *c* oxidase, Chem. Rev. 118 (2018) 2469–2490.
[5] P.R. Rich, Mitochondrial cytochrome *c* oxidase: catalysis, coupling and controversies, Biochem. Soc. Trans. 45 (2017) 813–829.
[6] J.F. Nagle, S. Tristram-Nagle, Hydrogen bonded chain mechanisms for proton conduction and proton pumping, J. Membr. Biol. 74 (1983) 1–14.
[7] T.E. Decoursey, Voltage-gated proton channels and other proton transfer pathways, Physiol. Rev. 83 (2003) 475–579.
[8] S. Iwata, C. Ostermeier, B. Ludwig, H. Michel, Structure at 2.8 ångstrom resolution of cytochrome *c* oxidase from *Paracoccus denitrificans*, Nature 376 (1995) 660.
[9] T. Tsukihara, H. Aoyama, E. Yamashita, T. Tomizaki, The whole structure of the 13-subunit oxidized cytochrome *c* oxidase at 2.8 ångstrom, Science 272 (1996) 1136.
[10] P. Brzezinski, R.B. Gennis, Cytochrome *c* oxidase: exciting progress and remaining mysteries, J. Bioenerg. Biomembr. 40 (2008) 521–531.
[11] R.J. Dodia, Structure-function Relationship of Mitochondrial Cytochrome *c* Oxidase: Redox Centres, Proton Pathways and Isozymes, in Ph.D. thesis, UCL (University College London), London, UK, 2014.
[12] A. Maréchal, F. Haraux, B. Meunier, P.R. Rich, Determination of H+/e ratios in mitochondrial yeast cytochrome *c* oxidase, BBA-Bioenergetics, (2014) e100.
[13] B. Meunier, A. Maréchal, P.R. Rich, Construction of histidine-tagged yeast mitochondrial cytochrome *c* oxidase for facile purification of mutant forms, Biochem. J. 444 (2012) 199–204.
[14] A. Maréchal, et al., Channel mutations in yeast cytochrome *c* oxidase support a common pumping mechanism from bacteria to mitochondria, (in preparation).
[15] L. Florens, B. Schmidt, J. McCracken, S. Ferguson-Miller, Fast deuterium access to the buried magnesium/manganese site in cytochrome *c* oxidase, Biochemistry 40 (2001) 7491–7497.
[16] V.R. Kaila, V. Sharma, M. Wikström, The identity of the transient proton loading site of the proton-pumping mechanism of cytochrome *c* oxidase, Biochim. Biophys. Acta (BBA)-Bioenergetics 1807 (2011) 80–84.
[17] A.M. Hartley, N. Lukoyanova, Y. Zhang, A. Cabrera-Orefice, S. Arnold, B. Meunier, N. Pinotsis, A. Marechal, Structure of yeast cytochrome *c* oxidase in a supercomplex with cytochrome bc_1, Nat. Struct. Mol. Biol. 26 (2019) 78–83.
[18] T. Tsukihara, K. Shimokata, Y. Katayama, H. Shimada, K. Muramoto, H. Aoyama, M. Mochizuki, K. Shinzawa-Itoh, E. Yamashita, M. Yao, The low-spin heme of cytochrome *c* oxidase as the driving element of the proton-pumping process, Proc. Natl. Acad. Sci. 100 (2003) 15304–15309.
[19] S. Yoshikawa, A. Shimada, Reaction mechanism of cytochrome *c* oxidase, Chem. Rev. 115 (2015) 1936–1989.
[20] M. Wikström, V. Sharma, V.R. Kaila, J.P. Hosler, G. Hummer, New perspectives on proton pumping in cellular respiration, Chem. Rev. 115 (2015) 2196–2221.
[21] A. Shimada, M. Kubo, S. Baba, K. Yamashita, K. Hirata, G. Ueno, T. Nomura, T. Kimura, K. Shinzawa-Itoh, J. Baba, K. Hatano, Y. Eto, A. Miyamoto, H. Murakami, T. Kumasaka, S. Owada, K. Tono, M. Yabashi, Y. Yamaguchi, S. Yanagisawa, M. Sakaguchi, T. Ogura, R. Komiya, J. Yan, E. Yamashita, M. Yamamoto, H. Ago, S. Yoshikawa, T. Tsukihara, A nanosecond time-resolved XFEL analysis of structural changes associated with CO release from cytochrome *c* oxidase, Sci. Adv. 3 (2017) e1603042.
[22] I. Ishigami, N.A. Zatsepin, M. Hikita, C.E. Conrad, G. Nelson, J.D. Coe, S. Basu, T.D. Grant, M.H. Seaberg, R.G. Sierra, M.S. Hunter, P. Fromme, R. Fromme, S.-R. Yeh, D.L. Rousseau, Crystal structure of CO-bound cytochrome *c* oxidase determined by serial femtosecond X-ray crystallography at room temperature, Proc. Natl. Acad. Sci. 114 (2017) 8011–8016.
[23] N. Yano, K. Muramoto, A. Shimada, S. Takemura, J. Baba, H. Fujisawa, M. Mochizuki, K. Shinzawa-Itoh, E. Yamashita, T. Tsukihara, The Mg^{2+} – containing water cluster of mammalian cytochrome *c* oxidase collects four pumping proton equivalents in each catalytic cycle, J. Biol. Chem. 291 (2016) 23882–23894.
[24] S. Yoshikawa, K. Shinzawa-Itoh, R. Nakashima, R. Yaono, E. Yamashita, N. Inoue, M. Yao, M.J. Fei, C.P. Libeu, T. Mizushima, Redox-coupled crystal structural changes in bovine heart cytochrome *c* oxidase, Science 280 (1998) 1723–1729.
[25] V. Sharma, P.G. Jambrina, M. Kaukonen, E. Rosta, P.R. Rich, Insights into functions of the H channel of cytochrome *c* oxidase from atomistic molecular dynamics simulations, Proc. Natl. Acad. Sci. 114 (2017) E10339–E10348 (201708628).
[26] P.R. Rich, A.J. Moody, Cytochrome *c* oxidase, in: P. Gräber, G. Milazzo (Eds.), Bioenergetics, Birkhäuser-Verlag AG Basel, 1997, pp. 418–456.
[27] R. Dodia, B. Meunier, C.W. Kay, P.R. Rich, Comparisons of subunit 5A and 5B isoenzymes of yeast cytochrome *c* oxidase, Biochem. J. 464 (2014) 335–342.
[28] A.J. Moody, P.R. Rich, The effect of pH on redox titrations of haem a in cyanide-liganded cytochrome *c* oxidase: experimental and modelling studies, Biochim. Biophys. Acta (BBA)-Bioenergetics 1015 (1990) 205–215.
[29] D. Blair, W.R. Ellis, H. Wang, H. Gray, S. Chan, Spectroelectrochemical study of cytochrome *c* oxidase: pH and temperature dependences of the cytochrome potentials. Characterization of site-site interactions, J. Biol. Chem. 261 (1986) 11524–11537.
[30] A. Maréchal, B. Meunier, D. Lee, C. Orengo, P.R. Rich, Yeast cytochrome *c* oxidase: a model system to study mitochondrial forms of the haem–copper oxidase superfamily, Biochim. Biophys. Acta (BBA)-Bioenergetics 1817 (2012) 620–628.
[31] S. Rathore, J. Berndtsson, L. Marin-Buera, J. Conrad, M. Carroni, P. Brzezinski, M. Ott, Cryo-EM structure of the yeast respiratory supercomplex, Nat. Struct. Mol. Biol. 26 (2019) 50.
[32] J. Lee, X. Cheng, J.M. Swails, M.S. Yeom, P.K. Eastman, J.A. Lemkul, S. Wei, J. Buckner, J.C. Jeong, Y. Qi, CHARMM-GUI input generator for NAMD, GROMACS, AMBER, OpenMM, and CHARMM/OpenMM simulations using the CHARMM36 additive force field, J. Chem. Theory Comput. 12 (2015) 405–413.
[33] M.P. Johansson, V.R. Kaila, L. Laakkonen, Charge parameterization of the metal centers in cytochrome *c* oxidase, J. Comput. Chem. 29 (2008) 753–767.
[34] V. Sharma, K.D. Karlin, M. Wikström, Computational study of the activated O_H state in the catalytic mechanism of cytochrome *c* oxidase, Proc. Natl. Acad. Sci. 110 (2013) 16844–16849.
[35] A.D. MacKerell Jr.et al., All-atom empirical potential for molecular modeling and dynamics studies of proteins, J. Phys. Chem. B 102 (1998) 3586–3616.
[36] J.B. Klauda, R.M. Venable, J.A. Freites, J.W. O'Connor, D.J. Tobias, C. Mondragon-Ramirez, I. Vorobyov, A.D. MacKerell Jr, R.W. Pastor, Update of the CHARMM all-atom additive force field for lipids: validation on six lipid types, J. Phys. Chem. B 114 (2010) 7830–7843.
[37] H.J. Berendsen, J.v. Postma, W.F. van Gunsteren, A. DiNola, J. Haak, Molecular dynamics with coupling to an external bath, J. Chem. Phys. 81 (1984) 3684–3690.
[38] S. Nosé, A unified formulation of the constant temperature molecular dynamics methods, J. Chem. Phys. 81 (1984) 511–519.
[39] W.G. Hoover, Canonical dynamics: equilibrium phase-space distributions, Phys. Rev. A 31 (1985) 1695–1697.
[40] M.J. Abraham, T. Murtola, R. Schulz, S. Páll, J.C. Smith, B. Hess, E. Lindahl, GROMACS: high performance molecular simulations through multi-level parallelism from laptops to supercomputers, SoftwareX 1 (2015) 19–25.
[41] B. Hess, P-LINCS: a parallel linear constraint solver for molecular simulation, J. Chem. Theory Comput. 4 (2008) 116–122.
[42] M. Parrinello, A. Rahman, Polymorphic transitions in single crystals: a new molecular dynamics method, J. Appl. Phys. 52 (1981) 7182–7190.
[43] W. Humphrey, A. Dalke, K. Schulten, VMD: visual molecular dynamics, J. Mol. Graph. 14 (1996) 33–38.
[44] M.H. Olsson, C.R. Søndergaard, M. Rostkowski, J.H. Jensen, PROPKA3: consistent treatment of internal and surface residues in empirical pKa predictions, J. Chem.

Theory Comput. 7 (2011) 525–537.
[45] B. Meunier, C. Ortwein, U. Brandt, R.P. Rich, Effects of mutation of residue I67 on redox-linked protonation processes in yeast cytochrome *c* oxidase, Biochem. J. 330 (1998) 1197–1200.
[46] B. Chance, G. Williams, Respiratory enzymes in oxidative phosphorylation III. The steady state, J. Biol. Chem. 217 (1955) 409–428.
[47] D. Han, A. Namslauer, A. Pawate, J.E. Morgan, S. Nagy, A.S. Vakkasoglu, P. Brzezinski, R.B. Gennis, Replacing Asn207 by aspartate at the neck of the D channel in the aa_3-type cytochrome *c* oxidase from *Rhodobacter sphaeroides* results in decoupling the proton pump, Biochemistry 45 (2006) 14064–14074.
[48] U. Pfitzner, K. Hoffmeier, A. Harrenga, A. Kannt, H. Michel, E. Bamberg, O.-M. Richter, B. Ludwig, Tracing the D-pathway in reconstituted site-directed mutants of cytochrome *c* oxidase from *Paracoccus denitrificans*, Biochemistry 39 (2000) 6756–6762.